NAVAL POSTGRADUATE SCHOOL

MONTEREY, CALIFORNIA

THESIS

SHOCK PROPAGATION IN SOFT GRANULAR MATERIALS

by

Anthony D. Severson

June 2019

Thesis Advisor:	Abram H. Clark IV
Second Reader:	James H. Luscombe

THIS PAGE INTENTIONALLY LEFT BLANK

REPORT DOCUMENTATION PAGE	*Form Approved OMB No. 0704-0188*

1. AGENCY USE ONLY *(Leave blank)*	**2. REPORT DATE** June 2019	**3. REPORT TYPE AND DATES COVERED** Master's thesis

4. TITLE AND SUBTITLE SHOCK PROPAGATION IN SOFT GRANULAR MATERIALS	**5. FUNDING NUMBERS**
6. AUTHOR(S) Anthony D. Severson	
7. PERFORMING ORGANIZATION NAME(S) AND ADDRESS(ES) Naval Postgraduate School Monterey, CA 93943-5000	**8. PERFORMING ORGANIZATION REPORT NUMBER**
9. SPONSORING / MONITORING AGENCY NAME(S) AND ADDRESS(ES) N/A	**10. SPONSORING / MONITORING AGENCY REPORT NUMBER**

11. SUPPLEMENTARY NOTES The views expressed in this thesis are those of the author and do not reflect the official policy or position of the Department of Defense or the U.S. Government.

12a. DISTRIBUTION / AVAILABILITY STATEMENT Approved for public release. Distribution is unlimited.	**12b. DISTRIBUTION CODE** A

13. ABSTRACT (maximum 200 words)

Shock propagation in particulate materials is governed by the nonlinear interactions between particles. Spherical elastic particles have Hertzian contacts, meaning that they effectively interact via nonlinear springs. Hertzian interactions give rise to nonlinear wave behavior, which has been studied extensively for 1D chains of spheres (e.g., Newton's cradle), where energy is transmitted perfectly from one particle to the next and the internal sound speed of a particle is assumed to be quasi-infinite. In more realistic situations, forces do not propagate along a single network, but along force chains, which are spatially anistotropic structures that transmit stress. Additionally, shocks can propagate at speeds similar to the internal sound speed.

Through shock experiments on 2D assemblies of frictional, photoelastic disks, we show three key results: (1) Two distinct wave speeds emerge after impact, one of which represents the primary force propagation wave; (2) this force propagation speed scales (as a power law) with the intruder velocity can indeed approach the characteristic sound speed inside a grain; and (3) in the shock regime, these propagation speeds are independent of confining pressure and fall along a single branch.

14. SUBJECT TERMS granular material, nonlinear force propagation, power law scaling	**15. NUMBER OF PAGES** 53
	16. PRICE CODE

17. SECURITY CLASSIFICATION OF REPORT	**18. SECURITY CLASSIFICATION OF THIS PAGE**	**19. SECURITY CLASSIFICATION OF ABSTRACT**	**20. LIMITATION OF ABSTRACT**
Unclassified	Unclassified	Unclassified	UU

NSN 7540-01-280-5500 Standard Form 298 (Rev. 2-89) Prescribed by ANSI Std. 239-18

THIS PAGE INTENTIONALLY LEFT BLANK

Approved for public release. Distribution is unlimited.

SHOCK PROPAGATION IN SOFT GRANULAR MATERIALS

Anthony D. Severson
Captain, United States Army
BAAS, Texas State University - San Marcos, 2012

Submitted in partial fulfillment of the
requirements for the degree of

MASTER OF SCIENCE IN APPLIED PHYSICS

from the

NAVAL POSTGRADUATE SCHOOL
June 2019

Approved by: Abram H. Clark IV
Advisor

James H. Luscombe
Second Reader

Kevin B. Smith
Chair, Department of Physics

THIS PAGE INTENTIONALLY LEFT BLANK

ABSTRACT

Shock propagation in particulate materials is governed by the nonlinear interactions between particles. Spherical elastic particles have Hertzian contacts, meaning that they effectively interact via nonlinear springs. Hertzian interactions give rise to nonlinear wave behavior, which has been studied extensively for 1D chains of spheres (e.g., Newton's cradle), where energy is transmitted perfectly from one particle to the next and the internal sound speed of a particle is assumed to be quasi-infinite. In more realistic situations, forces do not propagate along a single network, but along force chains, which are spatially anistotropic structures that transmit stress. Additionally, shocks can propagate at speeds similar to the internal sound speed.

Through shock experiments on 2D assemblies of frictional, photoelastic disks, we show three key results: (1) Two distinct wave speeds emerge after impact, one of which represents the primary force propagation wave; (2) this force propagation speed scales (as a power law) with the intruder velocity can indeed approach the characteristic sound speed inside a grain; and (3) in the shock regime, these propagation speeds are independent of confining pressure and fall along a single branch.

THIS PAGE INTENTIONALLY LEFT BLANK

TABLE OF CONTENTS

THIS PAGE INTENTIONALLY LEFT BLANK

LIST OF FIGURES

THIS PAGE INTENTIONALLY LEFT BLANK

I. INTRODUCTION

Granular materials are spatially disordered systems that respond in complex ways to disturbances. The study of impact into a granular medium continues to gain considerable interest and has particular relevance to military applications. Granular material physics is highly prevalent in kinetic military action through applications such as defensive gabions (commonly known as HESCO barriers), ground penetration of ordinance, engineering or mobility challenges on loose soil, and various other scenarios. While much progress has been made in the field there is still a great deal that is not well understood about force propagation in granular media, specifically at the grain scale. Multiple sources of nonlinearity make it difficult to accurately describe grain-grain interactions when force is applied to a system.

Granular media contain multiple sources of nonlinearity, most notably the Hertzian-like contacts between individual grains. Hertzian contacts exhibit a non-trivial power law scaling between the contact force, f and particle deformation, δ where $f \propto \delta^{\alpha}$. The scaling exponent α is based on particle geometry where pure 'Hertzian' contacts are defined as $\alpha = 1.5$ [1], [2]. For quasi-2D systems this exponent, α is also greater than one, which differs from the linear ($\alpha = 1$) response expected for literal 2D systems. Since the characteristic 'stiffness' between grains relates changes in force with deformation (or in pressure with volume), it is often constant for 2D systems, as in a linear spring. However, in Hertzian contacts, where $\alpha \neq 1$, this stiffness is not constant (because $\frac{\partial f}{\partial \delta}$ or $\frac{\partial P}{\partial V}$ are not constant), meaning that the system increasingly stiffens as force is applied. Another major source of nonlinearity is that in a granular medium, forces propagate along spatially inhomogeneous networks known as force chains. This causes forces to propagate in irregular patterns rather than as a uniform wave front. Other sources of nonlinearity include the friction between grains and the fact that grain contacts are free to break apart. The combination of these complex factors make it difficult to accurately describe how forces propagate in disordered granular systems. The result is that non-linear scaling laws arise based on a variety of different factors such as material parameters, packing/confinement conditions, and impact parameters. In this thesis we build on previous work done in the

field by conducting experiments on quasi-2D system of granular materials. Specifically, we identify previously unstudied conditions and examine whether shock scaling adheres to existing theoretical and experimentally based models.

II. BACKGROUND

Through extensive study of impacts into a granular medium, foundational models have been developed, tested, and refined. Yet much is still not well understood about force propagation at the grain scale level. In this chapter we will define the problem and detail the evolution of these models by examining results of specific past work. We begin by exploring the complexities of granular materials and their inherent nonlinearity. Next, we examine a 1D case which can be solved analytically and serves as a theoretical basis for subsequent work. This model is then expanded to 2D and 3D by detailing past simulation and experimental work. Finally, we analyze limitations of this existing work to identify previously unstudied regimes, and define experimental parameters to study their response and agreement with predictions based on existing scaling laws.

A. COMPLEXITIES OF GRANULAR MATERIALS

Granular materials present a complex system where the dynamics of a bulk medium can in some cases behave like entirely different states of matter. When impacted, disorganized systems of grains are capable of supporting force waves. These waves can travel through the bulk with a characteristic velocity, strain and internal pressure, just as they would in a solid or a liquid. However, a few key differences arise in the response of granular materials versus other types of matter. First, in a granular medium these force waves propagate along spatially inhomogeneous networks of particles that are in direct contact. These force chains cause the wave to move in irregular patterns, rather than as a uniform wave front as would be expected in a typical crystalline lattice material. Furthermore, Hertzian contacts between individual grains can cause resulting force waves to be highly nonlinear. Figure 1 graphically depicts a nonlinear spring model which can be used to represent Hertzian interactions, where contact forces scale nonlinearly with compression. From this we note two distinct regimes of interest for propagating forces. The first is where the internal wave pressure is much smaller than the external pressure in which grains are confined. In this regime, for small deviations along the curve, the slope (or $\frac{\partial f}{\partial \delta}$) is relatively constant and therefore a linear approximation would be valid. The second (and

more interesting) case is the "shock" regime where the internal wave pressure is much larger than the confining pressure. In this regime, even for small deviations along the curve, the slope is not constant and linear approximations break down. As a result, nonlinearity dominates and forces propagate through the material as a supersonic shock wave. This is the regime our research focuses on. Finally, densely packed granular materials are capable of simultaneously supporting non-uniform stresses along different spatial dimensions. Work performed by da Cruz et al. develops an effective friction coefficient μ^* which characterizes a granular system's ability to support a shear stress without flowing. They examine how μ^* the effective friction coefficient of the material, depends on μ_g, the coefficient of friction between grains. They find that for frictional grains, the effective frictional coefficient is approximately 0.3, with little dependence on μ_g [3].

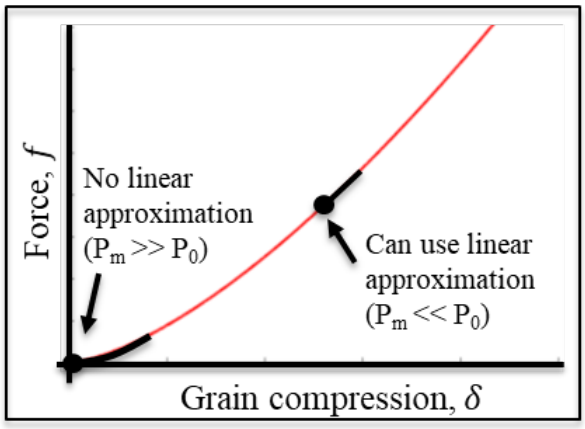

This figure depicts the nonlinear scaling relation between contact forces and grain compression that arises from Hertzian contacts.

Figure 1. Non-linear spring model

B. NONLINEARITY IN GRANULAR MATERIALS

Although multiple sources of nonlinearity exist in granular systems, the dominant mechanism is the contacts between individual grains. In a 2011 paper, Owens and Daniels detail the power law scaling for the contact force between two particles as where δ is the distance each particle is compressed and α is an exponent that depends on particle geometry. Hertzian contact theory is defined by the power law scaling of forces between

grains ($f \propto \delta^{\alpha}$) where $\alpha = 1.5$ for 3D spheres [4]. In literal 2D systems, this force scaling is expected to be linear where $\alpha = 1$. However, although it is not understood why, in quasi-2D systems (such as short cylinders or disks) this exponent, α tends to vary between 1.2 and 1.5. Therefore, Hertzian contact theory often serves as the primary basis for modeling interactions between grains, particularly the propagation of waves (such as sound) through a bulk medium. In the linear regime, waves propagate at the speed of sound in the medium. It can be shown that this sound velocity $c_0 \propto \sqrt{s}$ where *s,* the contact stiffness between grains, is equal to $\frac{\partial f}{\partial \delta}$. Since $\alpha \neq 1$ for Hertzian-like contacts, this characteristic stiffness is not constant, and therefore neither is c_0. Using these dependencies, we can derive a scaling relation between the sound velocity and contact force in the linear regime: where since $s \propto \delta^{\alpha-1} \propto f^{\frac{\alpha-1}{\alpha}}$ therefore implies that $c_0 \propto f^{\frac{\alpha-1}{2\alpha}}$. However, in the shock regime force waves propagate as a supersonic shock. Given that nonlinearity dominates this regime it is perhaps not surprising that the scaling of this wave speed can also be represented in terms of the power law exponent, α. Using the nonlinear force law and conservation of energy, Clark et al. developed a model relating collision time and force propagation speed. Through this model he detailed how the scaling of induced shock velocities can also be expressed in terms of $\alpha = 1$, where $V_s \propto u_p^{\frac{\alpha-1}{\alpha+1}}$, which we will subsequently show agrees with the results found in various simulations and experiments [5].

C. ANALYTICAL SOLUTION FOR 1D CASE

In studying a problem of this complexity, it is appropriate to begin with the simplest possible model, in this case a 1D chain of beads. 1D strongly nonlinear chains of beads permit the ability to tune the wave propagation from linear to nonlinear as studied by Daraio and Nesterenko et al. more than a decade ago. In the shock regime for a 1D case, they generate a nonlinear wave equation, Eq. (1) to describe particle displacement in the long wavelength limit [6]:

$$u_{tt} = -c^2 \left((-u_x)^{\frac{3}{2}} + \frac{a^2}{10} \{ (-u_x)^{\frac{1}{4}} [(-u_x)^{\frac{5}{4}}]_{xx} \} \right)_x, \quad (1)$$

where

$$-u_x > 0\,, \;\; c^2 = \frac{2E}{\pi\rho(1-\nu^2)}\,, \;\; c_0 = \left(\frac{3}{2}\right)^{\frac{1}{2}} c\, \xi_0^{\frac{1}{4}}\,.$$

This wave equation can be satisfied using a periodic cosine solution, Eq. (2) as shown below.

$$\xi = \left(\frac{5\,V_s^2}{4\,c^2}\right)^2 \cos^4\left(\frac{\sqrt{10}}{5a}x\right) \quad (2)$$

In the nonlinear regime, impacts produce a soliton wave that propagates through the material at some velocity V_s, which is generally much faster than the particle velocity, u_p. In the solution above we discover that the amplitude and velocity of the wave are strongly coupled (a hallmark of nonlinear waves). Experimental work shows that an initial wave emerges with an amplitude of higher order than subsequent secondary waves. This indicates that the wave can be considered as a soliton and therefore closely approximated using one hump of the periodic solution. This strain equation can be re-written using a Trigonometric expansion as:

$$\xi = \left(\frac{25}{16\,c^4}\right) V_s^4 \; \frac{1}{8}\left[3 + \cos\left(\frac{4\sqrt{10}}{5a}x\right) + 4\cos\left(\frac{2\sqrt{10}}{5a}x\right)\right].$$

We then examine the case of maximum strain and rearrange to produce an equation for the solitary wave speed. As shown below, the solitary wave speed V_s can then be expressed in terms of a normalized max strain, $\xi_r = \frac{\xi_m}{\xi_0}$ in Eq. (3):

$$V_s = c_0 \frac{1}{(\xi_r - 1)} \left(\frac{4}{15}\left[3 + 2\,\xi_r^{\frac{5}{2}} - 5\,\xi_r\right]\right)^{\frac{1}{2}} \quad (3)$$

or normalized force, $f_r = \frac{F_m}{F_0}$ in Eq. (4):

$$V_s = 0.9314 \left(\frac{4\,E^2\,F_0}{a^2\,\rho^3\,(1-\nu^2)^2}\right)^{\frac{1}{6}} \left(\frac{1}{(f_r^{2/3}-1)}\right) \left(\frac{4}{15}\left[3 + 2\,f_r^{\frac{5}{3}} - 5\,f_r^{\frac{2}{3}}\right]\right)^{\frac{1}{2}}. \quad (4)$$

In the limit where $F_m \gg F_0$, the solitary wave solution simplifies to:

$$V_s = \frac{2}{\sqrt{5}}\, c\, {\xi_m}^{\frac{1}{4}} = \left(\frac{16}{25}\right)^{\frac{1}{5}} c^{\frac{4}{5}}\, {u_p}^{\frac{1}{5}} = 0.68 \left(\frac{2E}{a\rho^{\frac{3}{2}}(1-\nu^2)}\right)^{\frac{1}{3}} {F_m}^{\frac{1}{6}}. \quad (5)$$

Using this result, they show that the shock wave speed can be expressed with a nonlinear dependence on maximum strain ξ_m, particle velocity u_p, and the maximum force between particles F_m [7], [8]. As expected, we find that Eq. 5 indeed shows that $V_s \propto {u_p}^{\frac{\alpha-1}{\alpha+1}}$ where α = 1.5 for spherical particles.

D. SIMULATIONS IN THE 2D CASE

Next we examine a two dimensional case by reviewing work done by Gomez et al. in which they developed simulations to model shock scaling in grains. They began by preparing a 2D Hertzian packing of frictionless spheres contained inside a fixed volume. A small average initial particle overlap $\delta_0 \sim P_0^{\frac{2}{3}}$ is introduced to simulate the bed being held at a fixed initial pressure. A piston then compresses the bed horizontally, moving at a continuous velocity u_p. Using Discrete Element Simulations, they numerically integrate Newton's equations of motion for systems of 10^3 to 10^4 particles with appropriate boundary conditions applied [9]. The results in Figure 2 show that as expected, distinguishable linear and shock regimes arise. Additionally, they show that the resulting shock speed scales nonlinearly with particle (or intruder) velocity in the shock regime.

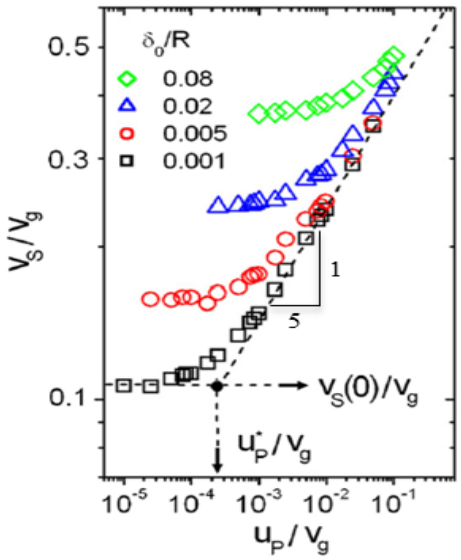

This figure depicts the shock velocity as a function of particle velocity for varying particle overlaps.

Figure 2. 2D simulation results by Gomez et al. Source: [9].

These results support two key conclusions previously derived in the 1D case: First, that different initial confining pressures are responsible for the emergence of two distinct (linear and shock) regimes. Second, in the shock regime, the resulting wave speed scales nonlinearly ($V_s \sim u_p^{\frac{1}{5}}$) with intruder velocity. This is again consistent with the expected result where $V_s \propto u_p^{\frac{\alpha-1}{\alpha+1}}$ with $\alpha = 1.5$ for spherical particles. It is also important to note how this solitary wave speed scales with changes in confining pressure. In the so-called linear regime, the wave speed increases as confining pressure increases. This scaling also appears relatively consistent with the expected scaling based on sound speed where $c_0 \propto f^{\frac{\alpha-1}{2\alpha}}$ ($\alpha = 1.5$). However, in the shock regime, the shock velocities appear independent of confining pressure and all fall on the same branch. This also appears to agree with the conclusions derived from the 1D solution, that in the limit where $F_m \gg F_0$ the dependence on confining pressure is negligible. Importantly, the results of the Gomez simulation work show the previously developed scaling relations are consistent between 1D and 2D systems.

E. EXPERIMENTS IN THE 2D CASE

Photoelastic disks have been used in multiple studies to experimentally explore 2D frictional systems of grains. In photoelasticity, the dielectric properties of a material depend on local stresses. These discs, when viewed through circular polarizers, can therefore capture microscopic data pertaining to the strain inside individual grains. Owens and Daniels used photoelastic disks in their work on sound propagation and the effects of forces chains in granular materials. By examining changes in image brightness, they were able to corroborate the power law scaling ($f \propto \delta^{\alpha}$) of Hertzian contact forces between grains. They assert that for these discs, α should fall between 1.0 (rectangular contacts between infinite co-planar cylinders) and 1.5 (for spheres). They conducted impact experiments in the linear regime where through data gathered from piezoelectric sensors, they estimate that α ≈ 5/4 [4]. Experimental work performed by Clark et al. also used photoelastic disks to study vertical intruder impacts into 2D systems of grains which were confined on the remaining three sides (top side unconfined). As shown in Figure 3, their results confirm that in the case of weak pre-confinement, a shock regime emerges where the induced wave speed scales nonlinearly with intruder velocity as $V_s \propto u_p{}^{\frac{\alpha-1}{\alpha+1}}$ [5]. For this agreement Clark's team estimated that α ≈ 1.4for these disks, which is reasonably close to Owens' estimate and falls comfortably in the expected range. However, they also observed that for very large impact velocities, the agreement of this scaling relation begins to break down as the ratio $\frac{V_s}{V_b}$ approaches roughly 0.8. The experimental data shows that above this threshold, shock velocities definitively trend upward for all three disk materials examine (varying material stiffness). They attribute this deviation to system confinement, and quantify it by fitting a (dotted) line using the existing scaling relation to this portion of the data, corresponding to $\alpha \approx 2.2$. This value for the power law exponent falls well outside the expected range, suggesting that the scaling behavior may change as shock speeds approach the bulk internal sound speed. Importantly we note that this result is not found in any of the other work we examined and is not predicted by the analytical model.

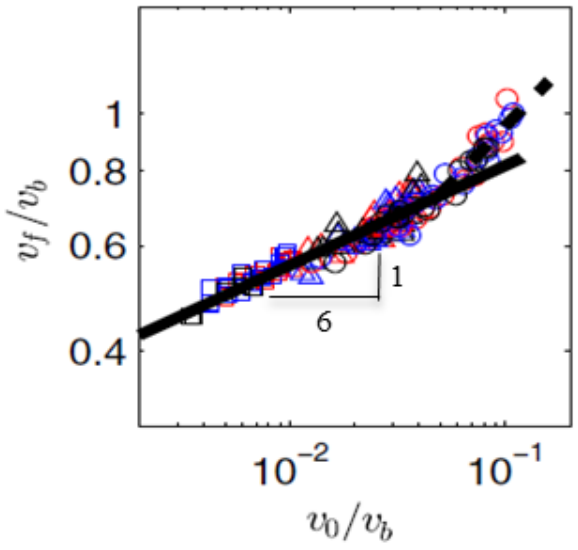

Figure 3. Experimental results by Clark et al. Source: [5].

F. EXPERIMENTS IN THE 3D CASE

We lastly expand these models to the three dimensional case by reviewing experimental work performed by Wildenberg et al. The team constructed an experimental apparatus housing a 3D bed of grains that allowed them to control application of a vertical confining pressure. A cylindrical plunger is affixed to one side and is free to slide into the bed through a circular hole. To carefully control the force applied at impact, a simple pendulum is used to strike the plunger with a heavy mass. Finally, pressure sensors and accelerometers are placed at two set locations (X_1 and X_2) inside the granular medium. These devices are used to measure the initial conditions, as well as the effects of impact inside the bulk [2]. They then conduct a series of experimental trials by varying the confining pressure and impact strength. The resulting wave speed is derived from time of flight measurements taken at the two embedded sensor locations to determine when the shock reaches the surrounding particles. They then calculate the impact strength, using the geometric mean of peak pressures measured at X_1 and X_2.

As shown in Figure 4, they again identify both linear and shock regimes resulting from variations in confining pressure. In the shock regime they again show that the wave speed scales nonlinearly ($V_s \sim F_m^{\frac{1}{6}}$) with impact strength [2]. This scaling relation is

consistent with the expected $V_s \propto F_m^{\frac{a-1}{2a}}$ (with $\alpha = 1.5$ for spherical particles) and again agrees with the theoretical prediction derived (Eq. 3) in the 1D case. We again note the wave velocity's dependence on confining pressure. In the linear regime, V_s again increases as confining pressure increases. However, the scaling does not appear consistent with the expected sound speed scaling where $c_0 \propto F_0^{\frac{a-1}{2a}}$. We also note that in the shock regime, confining pressure appears to be negligible. Though the data is quite noisy, it is reasonable to conclude that the shocks all fall generally on the same branch. This is again generally consistent with the 1D and 2D cases, but questions do remain about the data spread and the scaling behavior in the linear regime.

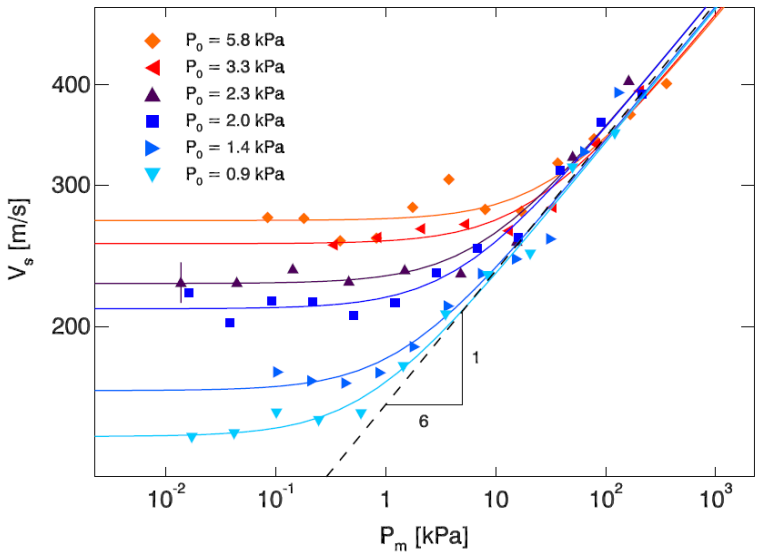

This figure depicts the shock velocity as a function of maximum internal wave pressure for a given range of initial confining pressures.

Figure 4. Experimental results by Wildenberg et al. Source: [2].

THIS PAGE INTENTIONALLY LEFT BLANK

III. RESEARCH FOCUS

In this section we outline the development of our experimental focus and define specific questions our research seeks to answer. First, we identify potential limitations of the past work outlined above to help inform our choice experimental parameters and setup. We then define new experimental parameters to study their response and agreement with predictions based on existing scaling laws. Finally, we detail three specific research questions our experiments seek to answer.

A. LIMITATIONS OF PREVIOUS STUDY

Finally, we identify a few key limitations to past simulations and experimental work in an effort to define new experimental parameters for study. First, the Gomez group's 2D simulations dealt only with frictionless grains which will not necessarily reproduce realistic, physical results. Additionally, these simulations don't include particle deformation but rather use "particle overlaps" to simulate pressure and compression [9]. While this approach likely gets many aspects of the system correct, it is unclear if it adequately models the complexity of contact stiffening between grains. Furthermore, the 2D simulations represent the resulting shock wave as a (relatively) uniform wave front, rather than propagating along irregular force chains. Second, the 3D experimental work, performed by Wildenberg's team, is opaque and thus limits data collection in some ways. Data about the force wave is captured only at only two locations within the medium and relies solely on time-of-flight measurements between those specific locations to determine the wave speed [2]. Additionally, although the wave speed increases with confining pressure in the linear regime, the scaling appears much larger than expected. Since the wave speed depends heavily on sound speed in the linear regime, the expected scaling is $V_s \propto c_0 \propto F_o^{\frac{1}{6}}$, which would produce smaller variations than those depicted. While the scaling in the shock regime appears consistent with existing models, the data is not compact and questions remain about the behavior across the complete data set. Finally, the 2D experimental work by Clark et al. is somewhat limited because it is performed without confining pressure [5]. The work demonstrates the merits of using photoelastic particles to

obtain force information from inside individual grains and shows that the method can produce data that scales as expected. However, the use of a variety of confining pressures and a wide range of impact velocities is desirable. Identifying these limitations of past work, we are then able to design an experiment that examines untested parameters and study their adherence to existing models.

B. EXPERIMENTAL PARAMETERS

Parameters are carefully chosen to ensure that the data collected spans a broad range of conditions and produce an experimental system that is unique from those outlined in previous study. First, we choose soft particles to determine whether existing models hold even when grains can be significantly deformed by initial confinement or impact force. Additionally, this allows us to study a regime where the bulk sound speed inside a grain is predicted to be small and therefore impact and shock velocities are expected to be similar in order of magnitude. This regime appears to be previously unstudied and while uncommon in many applications, has relevance in certain military scenarios involving high velocity impacts on materials. The bulk sound speed of a grain scales as $V_b \propto \sqrt{\frac{\varepsilon^*}{\rho}}$, where ε^* is the young's modulus and ρ is the mass density of the material from which the particles are constructed. For the particles chosen, V_b can be approximated on the order of 48 meters per second $\left(V_b \sim \sqrt{\frac{3\ E6}{1.3\ E3}}\right)$. Second, in this regime, we study whether horizontal shock velocities adhere to previously developed scaling laws under a variety of vertical confining pressures. To adequately capture the effects, confining forces, which are applied by weights on top of the system, are varied across roughly one order of magnitude, with masses between 290 and 2330 grams. A plunger (m = 290 g) is inserted from above so that confining pressure is relatively evenly applied across the entire width (w = 0.305 m) of the grain bed. The plunger serves as the base confining pressure and applies roughly 2.95 kPa vertically to the bed of grains. Additional masses are placed on top of the plunger to achieve the desired confining pressures (1x – 2x – 4x – 8x). Third, we examine how wave speed scales depends on particle velocity by applying a broad range of impact velocities spanning more than one order of magnitude. A pendulum is used to generate predictable impacts to

the horizontal plunger by carefully controlling the deflection angle (and therefore the height) to generate desired plunger velocities $(u_p \sim \sqrt{2gh})$. To attempt to generate data in both the linear and shock regimes, two small deflections (2° - 4°) and three large deflections (10° - 20° - 30°) are chosen. We assume a perfectly inelastic collision between the pendulum and plunger, resulting in a range of expected particle velocities from 0.10 to 1.46 meters per second. These experimental parameters are then combined with the limitations of previous study outlined earlier in the chapter to develop a realistic 2D experimental model for study.

C. RESEARCH QUESTIONS

Utilizing these parameters, we construct an experiment to study four primary research questions: 1) How is shock scaling affected for soft, highly deformable particles; 2) Can previously developed shock scaling laws be corroborated under varying confining pressures; 3) What happens when impact or shock speeds are similar to the bulk interior sound speed of a grain; 4) Are we able to identify a linear regime in soft particles that allow significant deformation? Using these questions as a framework, we define our primary research goal. We seek to experimentally study the same geometry as past work using quasi-2D photoelastic disks and observe how shock behavior in frictional, deformable particles agrees with previously developed scaling models.

THIS PAGE INTENTIONALLY LEFT BLANK

IV. METHODOLOGY

Using photoelastic disks, high-speed video, and image processing techniques, we analyze impact induced shocks in a granular medium. The primary objective of our research is to experimentally study shock behavior in a two-dimensional system comprised of frictional, deformable particles. Using the limitations of previous study as outlined in the previous chapter, we develop a few key parameters for the experiment. First, frictional grains that allow significant particle deformation are chosen in an effort to model the most realistic physical case possible. Second, a variety of confining pressures (spanning ~ 1 order) are vertically applied to the bulk, perpendicular to the impact axis. Third, photoelastic particles are chosen because they allow us to capture grain scale, local stress information inside the particles themselves. Image processing techniques are leveraged allowing the entire system to be examined simultaneously as the wave propagates.

A. PHOTOELASTIC TECHNIQUE

Granular materials can be made up of different types of solid particles (like sand, beads, or nuts) that exhibit the same system wide behaviors. To experimentally study force propagation in a granular material, we select small cylinders (or disks) made from a photoelastic material. The primary reason photoelastic material is chosen is that its unique material properties allow quantitative force information to be captured inside individual grains. The dielectric properties of these materials depend on local stresses, resulting in the development of visible fringe patterns (when viewed with a circular polarizer) inside the grains as contact forces are applied externally. In a 2017 paper, Daniels details these concepts of photo elasticity and polarization, as well as the theoretical basis for various mathematical method used to quantify force information [10]. As shown in Figure 5, light is placed behind the disks and a circular polarizer (two layers composed of a linear polarizer and a quarter-wave plate) is applied in between, with the linear polarizing layer closest to the light source. Passing first through the linear polarizing layer, the light's electric (E) and magnetic (B) fields oscillate in phase, with the electric field aligned with the polarizer's orientation and both fields mutually orthogonal to the direction of propagation. The

quarter-wave plate layer is constructed of carefully chosen *birefringent* material, meaning that inside the material, fast and slow directions for light propagation emerge as a result of the crystalline axis structure. The quarter-wave plate is aligned so that its fast axis is rotated ±45° relative to the orientation of the linear polarizer. The result is that in this circularly polarized light, the E fields along the fast and slow axis now oscillate 90° out of phase relative to each other. The light then passes through the disk and then through a second circular polarizer (oriented opposite the first and rotated 90°) before being captured by the camera.

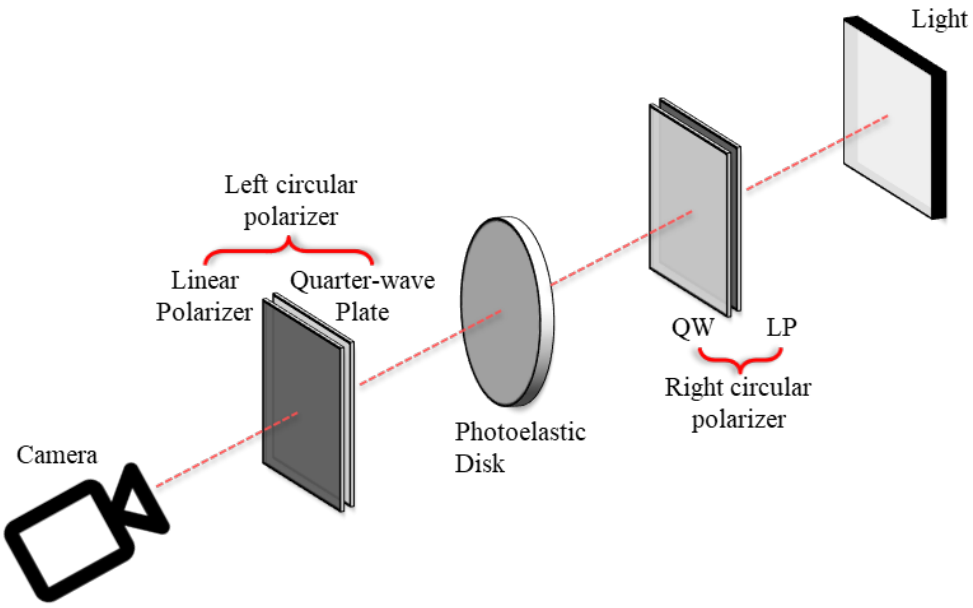

Figure 5. Schematic diagram of a setup using circular polarized light

As shown in Figure 6, the result of this process is that as force is applied to the particle, light and dark fringes appear inside the disk, where the patterns and intensity of light depend on the magnitude and direction of the force. This response allows us to quantitatively measure forces inside the grains themselves using various image processing techniques. A number of other considerations also support the use of photoelastic disks, including: 1) The edges of these disks are frictional and resist slipping, allowing them to construct system spanning networks that resist flow. 2) Disks can be constructed of

photoelastic materials which range from hard to soft, allowing for grains with varying degrees of compressibility. 3) Disks of varying diameter can be constructed, resulting in a disordered system which resists the formation of crystalline lattice structures. Therefore, we choose to study soft particles of varying diameters, constructed from photoelastic material.

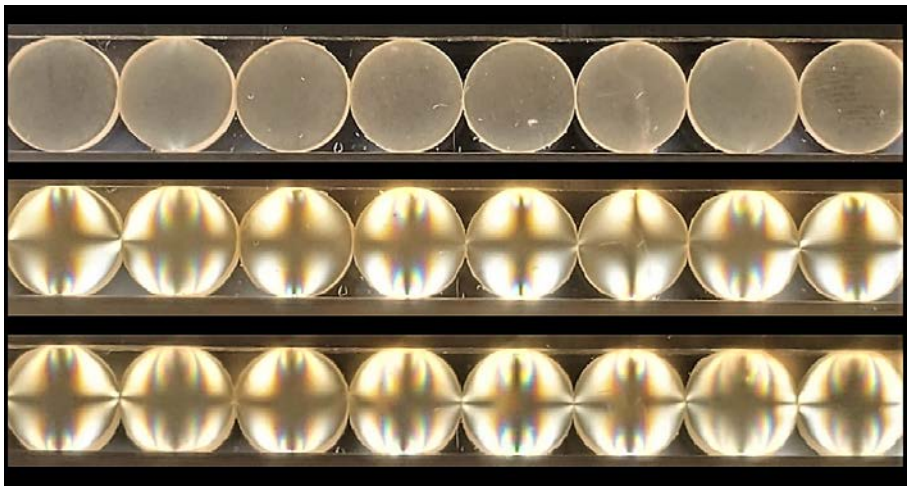

Figure 6. Image of photoelastic disks viewed using circular polarization

B. EXPERIMENTAL CONSTRUCTION

To begin, we plan, construct, and test an experimental apparatus designed to study our primary research questions. As shown on Figure 7, a clear box which allows for back lighting and video capture is constructed to house a quasi-2D packing of photoelastic disks. In this case, the term quasi-2D represents a system comprised of a single layer of particles with a small, finite thickness and is therefore taken to be 2D. The primary structure of the box is comprised of two solid walls (0.5 m x 0.5 m) built from 12.5 mm acrylic. These panels are fastened parallel to each other and spaced 4.5 mm apart to house the 2D packing of grains. This spacing is sufficient to allow the disks (2.85 mm thick) to both compress and move freely without flipping or overlapping during impact. Two, solid pieces of aluminum are placed inside the box (on the bottom and at one end) to serve as fixed boundaries. The interior of the box (h = 0.265 m; w = 0.305 m) is filled to capacity with a mixture of disks with two different diameters (d = 6 & 9 mm). Combing particles of

different sizes produces a disordered system and prevents crystallization. An acrylic plunger (equal in width to the grain bed) is constructed to allow weights to be added and is placed inside the box from above. This plunger allows varying initial confining pressures to be applied vertically to the entire system. A second acrylic plunger (equal in height to the grain bed) is placed between the panels and affixed at one end of the box so that it is free to move and horizontally compress the grains. A pendulum (length = 1.32 m) is constructed and placed so that it impacts this plunger, applying an accurate and repeatable particle velocity to the grain bed. Finally, the box and pendulum are securely mounted to a large optical table to provide a stable platform and ensure the apparatus does not move during impact and video capture.

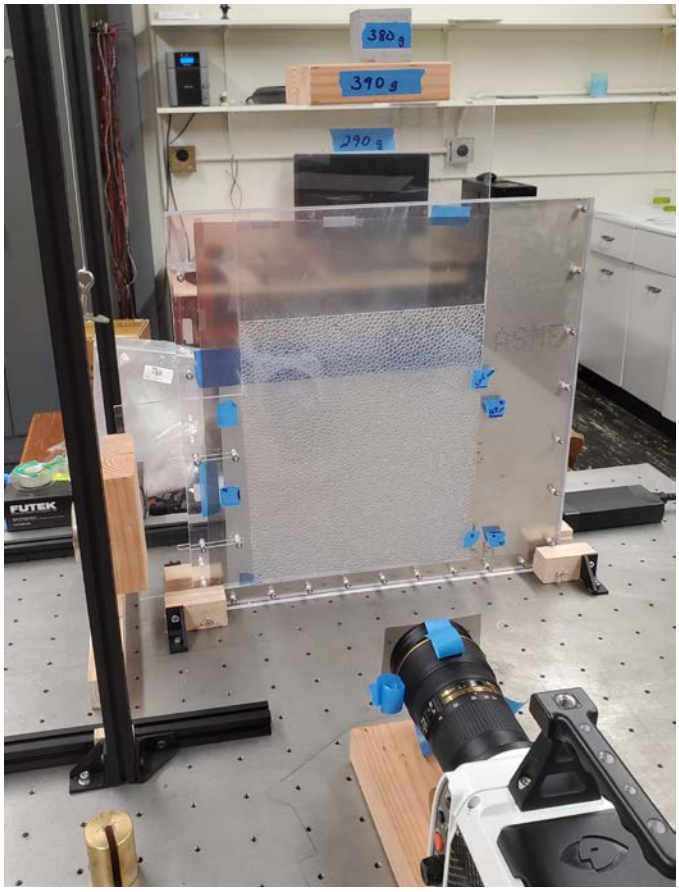

Figure 7. Experimental apparatus

C. DATA COLLECTION AND PROCESSING

Experimental data is collected via video taken with a Phantom v711 high speed camera and shot at 7,500 frames per second. The image resolution is set to 1200 x 800 pixels and focused on an area of the box measuring 308 mm wide by 205 mm tall. Therefore, the small and large particles translate (at roughly 4 pix per mm) to diameters of 24 and 36 pixels respectively. An LED light source and circular polarizers are positioned in front of and behind the box (according to the diagram in Figure 5) to allow for photoelastic imaging. The relatively high resolution allows us to in essence gather detailed, 'microscopic' data about the stress inside an individual grain. Each frame of the video is saved individually as 12-bit TIFF (Tagged Image File Format) images and then image processing is done using MATLAB software. Images are read in RGB (Red-Green-Blue) where the resulting 3D matrix (width x height x RBG value) represents the color and brightness of each pixel. The polarizers used are optimized for green light, so we select only this value, reducing the image matrix to 2D. A variety of techniques are applied during various phases of analysis to numerically capture how material stresses in the entire system change, frame by frame. The primary method involves comparing each frame after impact to the initial conditions by examining changes in the intensity values of each individual pixel. To capture details regarding how individual disks respond as force is applied, we apply a widely used photoelastic technique commonly known as the gradient squared or 'G^2' method. The theoretical basis for photoelastic models such as this are detailed extensively in work published in 2017 by Daniels et al. [10]. This method uses the square of the directional gradient to identify the fringe patterns inside the disk by comparing relative brightness values in each direction. Generating this G^2 value for each pixel in the frame, we subtract out the corresponding value from the initial frame before impact. This provides quantitative data depicting how much the inside of an individual grain has changed from its initial condition as a result of applied force. Using this method, we are able to track the progress of the force wave as it moves through the system. Since the intensity of light passing through the disk corresponds to applied, we sum the total brightness of each column to visibly depict the horizontal travel of the induced force wave. This is done for each frame and the resulting 1 x 1200 matrices are stacked to generate

plots that depict force propagation as shown in Figure 8. Since the data is plotted in space and time, a linear fit can easily be translated to a velocity for a given region of interest. Using these techniques, we are able to capture stress information across the entire system simultaneously, and evaluate how it changes frame by frame.

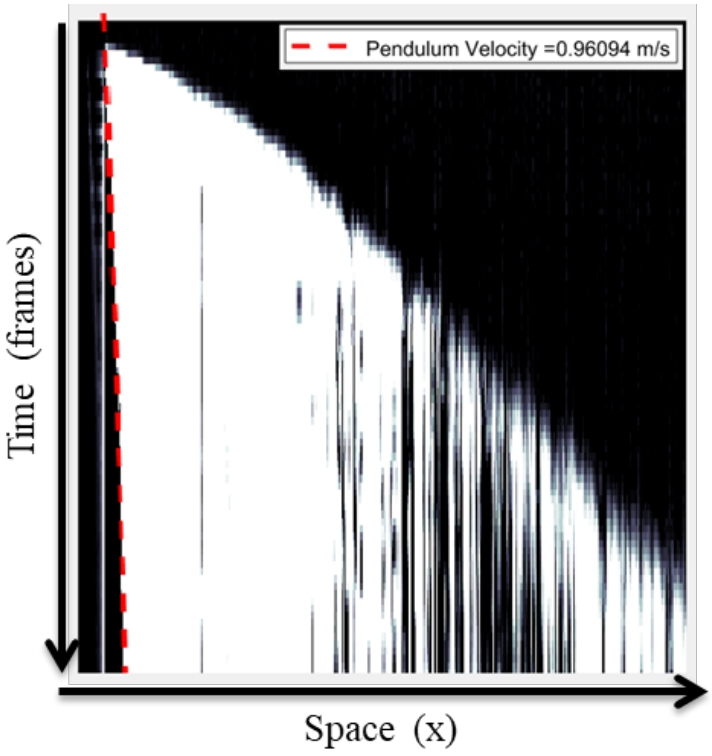

Figure 8. Sample 'space-time' plot produced through image processing

D. METHODOLOGY AND DATA VERIFICATION

Significant efforts are made to minimize error throughout the experimental process and are subsequently outlined in this section. The following three primary considerations are applied: 1) As previously outlined, the experimental apparatus was carefully constructed and is securely mounted to minimize external effects on the system. The spacing between the panels is carefully chosen to be sufficiently large to minimize friction between the disks and the wall, but not large enough for the disks to flip or overlap. 2) To minimize variance, five independent trials are conducted for each of the twenty sets of

experimental parameters. Following each impact, the plunger is removed, the grains are stirred, and the confining pressure is reapplied. This not only creates a unique system configuration for each trial but also ensures that no residual stresses remain from previous iterations. 3) A protractor is affixed to the pendulum, allowing for accurate, repeatable deflections to be applied. Consistency of the plunger velocity is confirmed using two methods. First, the front of the plunger is tracked over multiple frames and a time of flight measurement is used to determine its velocity. These velocities are verified as reasonable given the expected velocities outlined previously in the chapter. Second, since the plunger intrusion is visible in the space-time plots, a line corresponding to this velocity is overlaid on the plot and results in a satisfactory fit. Using this data, we calculate an average relative standard deviation of 7% across all 100 pendulum velocities considered. This is the only identifiable error we are able to calculate for the experiment and is not accounted for in any of our reported results. Based on these outlined considerations and the quantifiable error we have identified, the data analyzed in subsequent chapters is taken to be valid.

THIS PAGE INTENTIONALLY LEFT BLANK

V. DATA ANALYSIS

This chapter details the primary observations identified using the experimental methods and data processing outlined in the previous chapter. First, the 'space-time' plots reveal two distinct regimes that emerge after impact, where the associated wave speeds each possess different scaling properties.

A. ANALYSIS OF SPACE-TIME PLOTS

First, we develop 'space-time' plots (sample shown in Figure 8) to examine the system behavior over 100 experimental trials, spread evenly across 20 unique sets of experimental parameters (five trials per combination of confining pressure and impact velocity). Due to the photoelastic properties of the disks, the intensity of light captured on camera increases as additional stress is applied to the particle. Each frame is compared to the initial conditions to determine the change in brightness for every pixel (1200 x 800) in the image. These changes are then summed along the columns to create a single row vector (1200 x 1) depicting horizontal force propagation (in x) as increased light intensity. These row vectors are then stacked frame by frame (top to bottom) to create the 'space-time' plot which shows how the force wave progresses with time. It is also important to note that a limited number of frames (in our case < 50) are used to generate these plots in order to omit any effect of a rear boundary reflection.

Since these plots relate space and time, we can estimate a velocity using the slope of a line fit across a particular region $\left(m = \frac{\text{frames}}{\text{pixels}};\ V = \frac{1}{m} * \frac{\text{frames}}{\text{second}} * \frac{\text{meters}}{\text{pixel}}\right)$. As shown in Figure 9, two distinct regimes emerge in all of these plots. An initial regime corresponding to a fast wave speed develops after impact but is only visible for a very short time. (Note: flatter lines equal faster velocities because the axes are inverted.) We notice that the velocity of this initial wave appears relatively unchanged across all 20 sets of parameters, implying that it is independent of both impact velocity and confining pressure. Indeed, we notice that the red (dashed) line fits reasonably well across all four plots as the impact velocity and confining pressure vary. This is not an expected behavior for wave speeds in either the linear or the shock regime.

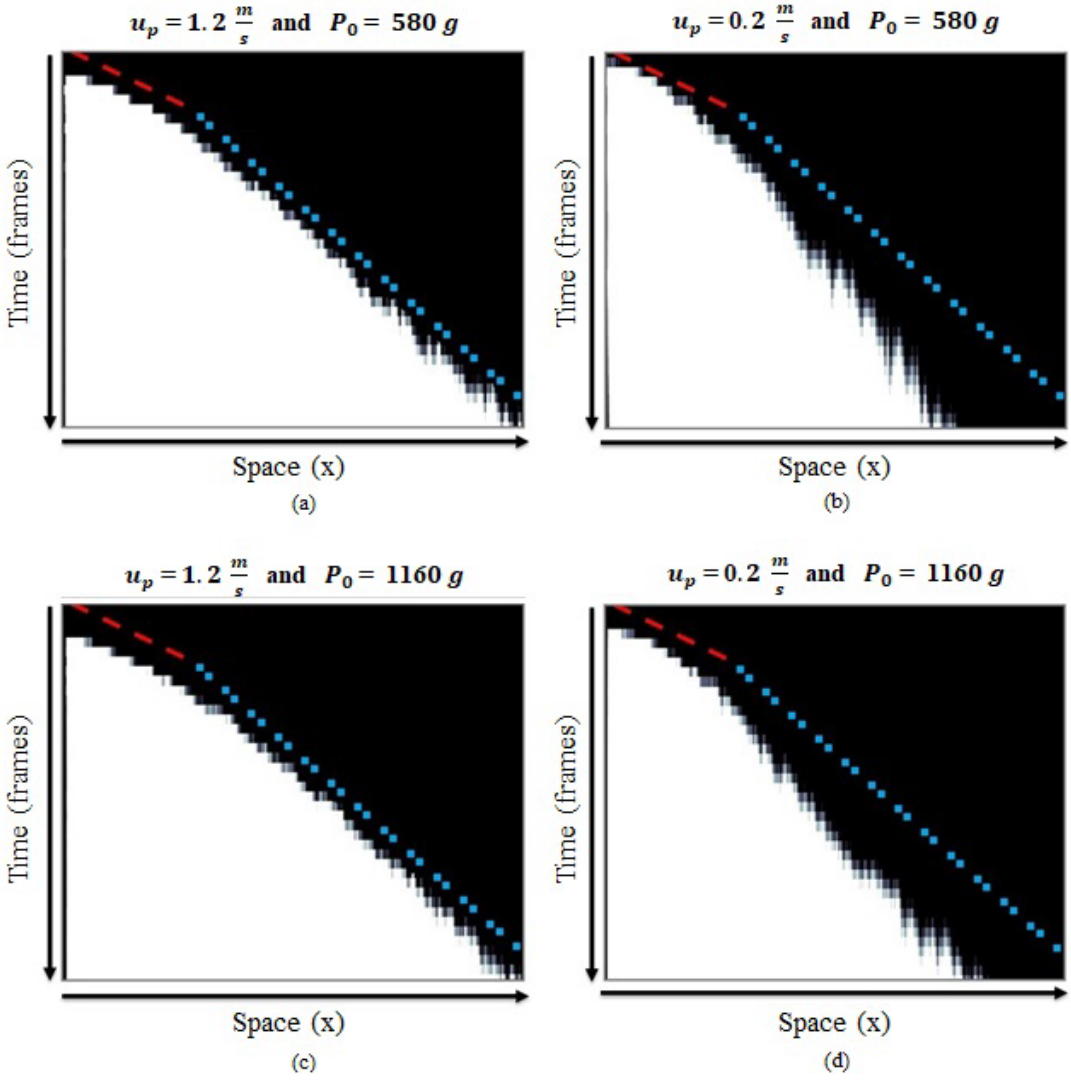

Figure 9. Comparison of 'space-time' plots for differing parameters

A second, more sustained regime emerges after only a few frames, corresponding with a slower velocity, though still on the same order as the initial wave. The wave speed in this regime changes with various experimental parameters, most noticeably increasing with intruder velocity. In Figure 9, the same blue (dotted) line is fit to all four plots. We notice that in plots (a) and (c), changes in confining pressure appear to have little to no impact on the fit of this line. However, when intruder velocity decreases as in plots (b) and

(d), the fit is clearly too fast, confirming that the speed of this wave indeed depends on u_p. This dependence is expected in the shock regime and suggests that this is the shock wave.

B. CALCULATING SHOCK VELOCITY

Given these observations, we next work to calculate the velocity of this wave to determine how it scales with impact velocity. Due to the wide disparity in range (and scale in terms of SI units) between the space and time axes, the linear fit method does not produce velocities accurate enough to consistently capture the relatively small shock scaling. Therefore, we use an alternate time of flight method to estimate the velocity and then verify it by fitting a line (using the corresponding slope) to the 'space-time' plot. For this method we again read in full 2D images frame by frame and isolate the green value of the image matrix to produce a raw image (as shown below). The force wave is then extracted using a comparison method similar to the one outlined in Methodology and plotted frame by frame (also shown below). As Figure 10 shows, although the force wave is visible in the raw images, the processed image provides a clear and detailed picture of the wave as it propagates through the system. This processing method allows us to accurately track how the wave advances frame by frame. This processed image also provides a stark visual representation of how waves propagate along the spatially inhomogeneous force chains discussed earlier. For many experimental parameters (most notably small impacts) the wave patterns are highly irregular, making it very difficult to characterize the 'front' of this non-uniform wave. Additionally, it is not possible to determine arbitrary thresholds in intensity that define the position of this front across all parameter sets. This directly contributes to a significant portion of the data noise present in the results.

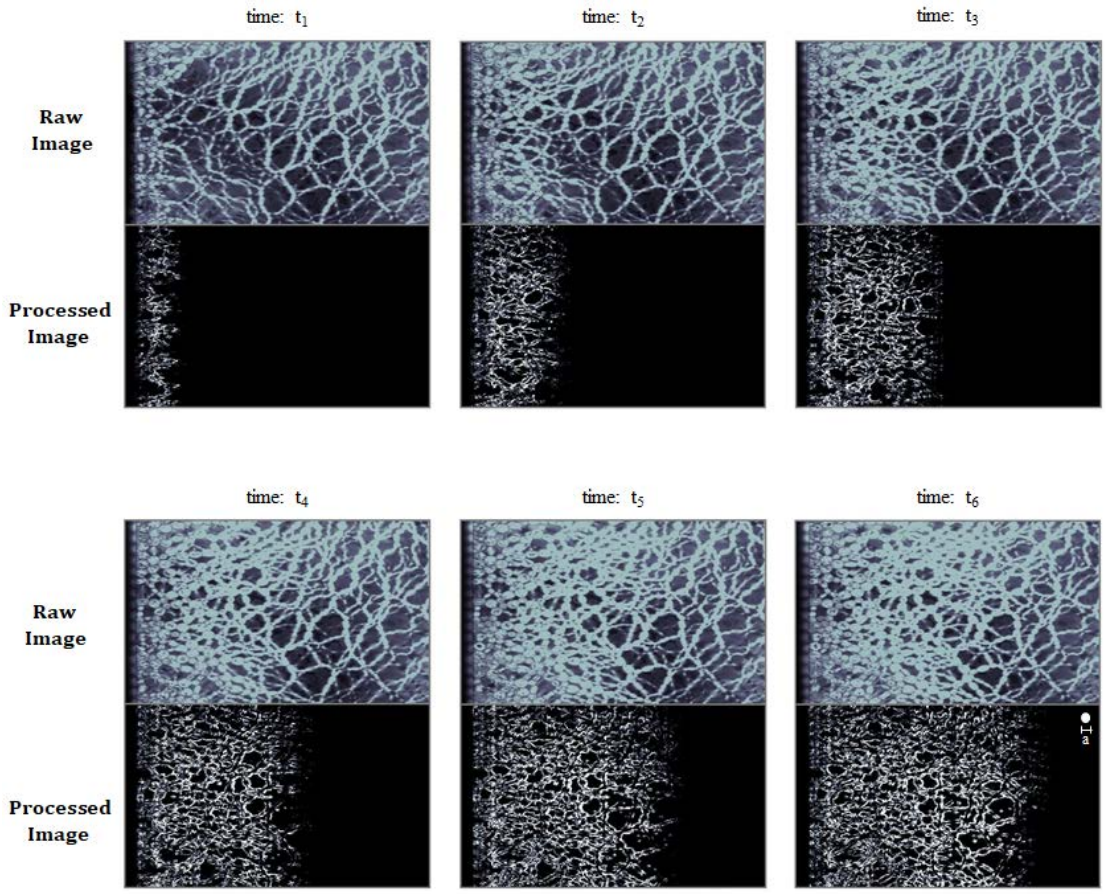

Figure 10. Sample of image processing performed to extract the wave front

Since the wave does not travel uniformly, we break the image into horizontal regions and track the progress of the defined wave front frame by frame. We then average these regions to attempt to minimize the effects of variance across the system and limit data noise as much as possible. Using this method, we calculate an average wave velocity across the entire system over the time steps corresponding to the second wave regime (identified previously in the 'space-time' plots). We then verify these velocities by fitting a line (with corresponding slope) to 'space-time' plots and confirm a reasonable agreement.

VI. RESULTS

Based on the observations of this data analysis, we identify four key results which are detailed in this chapter. First, we note that the wave speed identified in the initial regime is reasonably close to the first order prediction of the bulk sound speed inside these grains, suggesting that this may be what we see. Second, following this initial regime we identify wave speeds that exhibit the expected scaling, suggesting that the existing shock scaling models hold even for soft particles. Third, we further find that these shock speeds fall along a single branch, indicating that wave speeds are independent of confining pressure in the shock regime. Fourth, we are unable to clearly identify a linear regime in these soft, highly deformable particles. These results agree in many ways with the expected behavior based on past study, but also raise questions that we highlight for future study.

A. OBSERVATION OF INTERNAL SOUND SPEED

In examining the 'space-time' plots, we identify an initial regime with a corresponding fast wave speed that is briefly visible immediately after impact. This regime is typically only visible for roughly five or six frames, or less than 0.8 milliseconds after impact. Unexpectedly, we find that the corresponding wave speed in this regime appears to be largely independent of impact velocity or confining pressure. It is worth noting that these parameters seem to have some influence how long the regime is visible. In general, the regime remains visible slightly longer (and therefore deeper into the system) for both higher impact velocities and confining pressures. However, this initial regime is still very brief (roughly 10–15% in time length) relative to the sustained regime that follows it. Figure 11 shows that the same line (where $V_s \approx 58.5$ m/s) fits reasonably well in this regime across a broad range of experimental parameters. This initial regime is indicated on the figure by a blue (dotted) line placed at the fifth frame of each plot. Additionally, we note that this velocity is reasonably close to the expected internal sound speed in these soft particles. As previously shown, V_b is estimated to be on the order of 48 meters per second or $\left(V_b \propto \sqrt{\frac{\varepsilon^*}{\rho}} \sim C_1 \sqrt{\frac{3\ E6}{1.3\ E3}}\right)$ where C_1 is a constant of order unity. The internal sound speed is independent of impact velocity and only minimally affected by confining pressure, which

is consistent with the wave speed in this initial regime. We therefore conclude that the bulk internal sound speed may in fact be visible in these soft particles, though only for a short time.

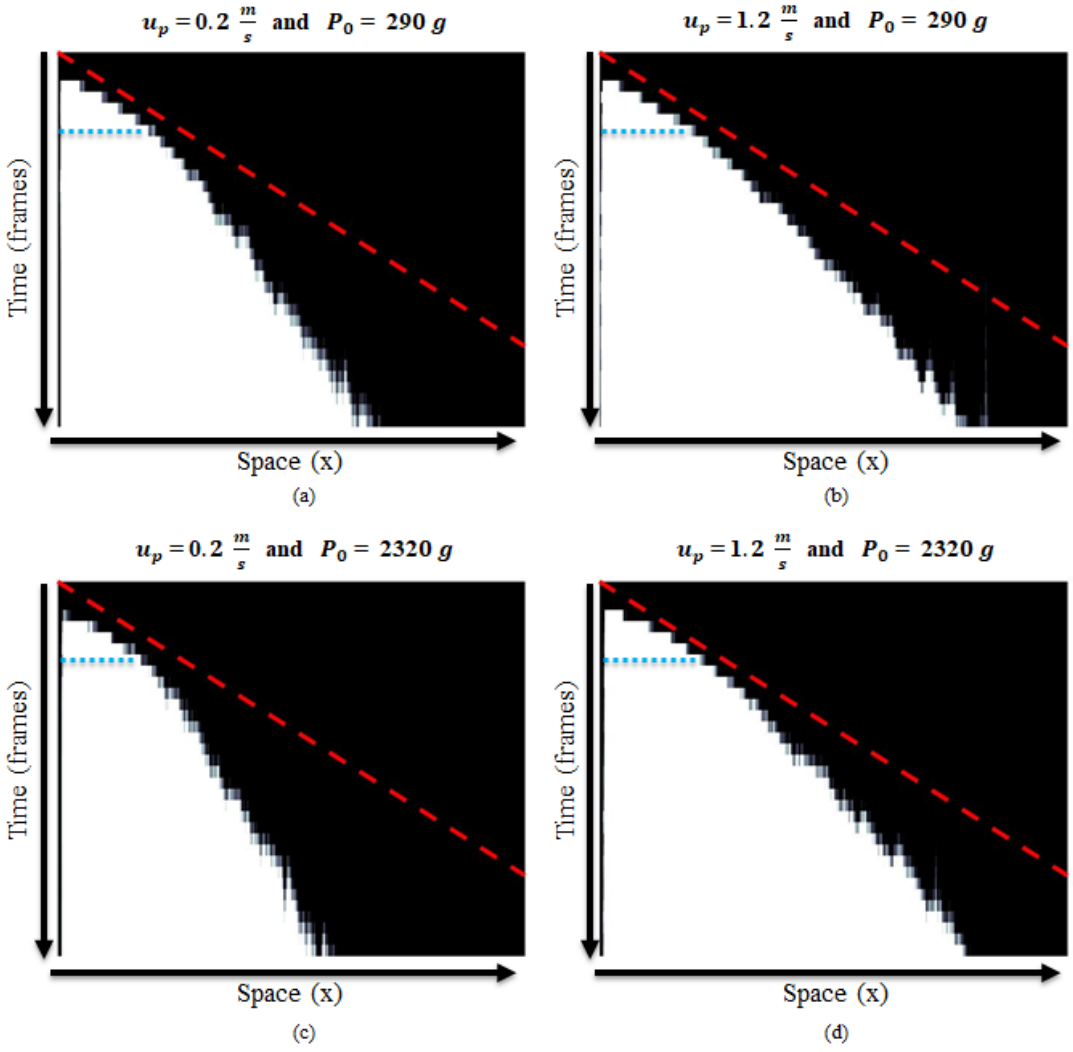

Figure 11. Internal sound speed fit for varying experimental parameters

B. SHOCK SCALING IN SOFT PARTICLES

The ‘space-time’ plots clearly reveal a sustained force propagation regime where the corresponding wave speed depends on impact velocity. This is an expected behavior in the nonlinear regime and our data analysis (detailed in the previous chapter) confirms that

this is indeed a shock induced by impact. We then analyze this shock scaling and determine its adherence to existing models. The shock velocities of the five independent trials are averaged for each of the twenty unique experimental parameters and then plotted as a function of impact velocity. Figure 12 shows a clear scaling relation between the induced shock speed and impact velocity. As shown previously, it is predicted that the shock speed scales with impact velocity as $V_s \propto u_p^{\frac{\alpha-1}{\alpha+1}}$, where α is the power law exponent and depends on particle geometry. Using the estimate from Clark et al. where $\alpha \approx 1.4$ for short cylinders, the shock scaling relation simplifies to $V_s \propto u_p^{\frac{1}{6}}$ and is also shown in the figure overlaying the experimental data [5].

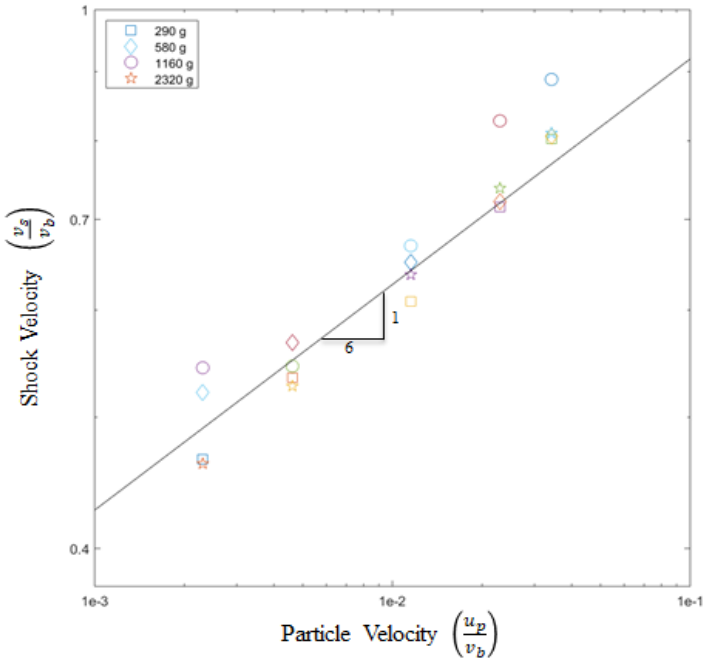

Figure 12. Shock scaling of quasi-2D experimental results

Although the data is somewhat noisy, these results indicate that the shock scaling model holds for soft, highly deformable particles. The figure in fact shows that the data is reasonably tight and closely follows the shock scaling model for moderate impact velocities (middle portion of the data). However, for small and large impacts, we find that the fit is adequate but contains significantly more variance. Small impacts applied to grains

under large initial confinement are difficult to capture when the image processing thresholds are set high enough to eliminate noise. Additionally, this portion of the data corresponds with a transition to the linear regime as we examine in a later section. Interestingly, the variance increases for large impacts in two different ways. First, the agreement for the third largest confinement deviates significantly, however we reasonably believe this to be an image processing artifact. The second and more interesting variance is that while three of the data points are tightly grouped for each of the two largest impacts, they sit noticeably above the trend line for the largest intruder velocity. This correlates with an observation made by Clark et al. in their 2015 quasi-2D experiment. For large impacts they also observed that the data begins to definitively trend upwards as the ratio of $\frac{V_s}{V_b}$ approaches roughly 0.8 [5]. This ratio threshold corresponds with our results, suggesting that the scaling behavior may in fact change as the shock speed approaches the bulk internal sound speed. Again we note that there is nothing in the analytical model that suggests this behavior and it is not observed in the other simulations and experimental results we previously outlined. However, since those results do not depict the internal sound speed there is no way to determine if the shock speeds they observe fall close to or above the threshold ratio. The replication of this unexpected behavior suggests that existing analytical and empirical scaling models may be incomplete and future study is needed.

C. IMPACTS OF INITIAL CONFINEMENT IN SHOCK REGIME

Previous simulations and experimental work show that the effects of initial confinement differ between the linear and shock regimes. As previously discussed, in the linear regime force waves along Hertzian contacts propagate at the sound speed and therefore depend on confining force $\left(c_0 \propto \sqrt{s} \propto {f_0}^{\frac{\alpha-1}{2\alpha}}\right)$. However, in the shock regime (where $f_0 \ll f_m$) the maximum contact force inside the wave dominates and the shock velocity is independent of initial confining force. We indeed confirm in Figures 2 - 4, all shock velocities in this regime fall along the same branch, regardless of confining pressure [5], [9] and [2]. As shown in Figure 12 our experimental data falls roughly along a single branch, further indicating that there is no systematic dependence on initial confinement in this shock regime. Given that the experimental data contains a reasonable amount of noise,

we again use a previous image processing technique to corroborate this conclusion. Holding impact velocity fixed, we track the force wave frame by frame for both the smallest and largest confining pressures tested. A sample of this comparison method is depicted in Figure 13 and confirms this wave speed is independent of initial confinement. Stacking these images, we clearly see there is no discernable difference in the wave progression, even when the confining pressures are separated by nearly an order of magnitude.

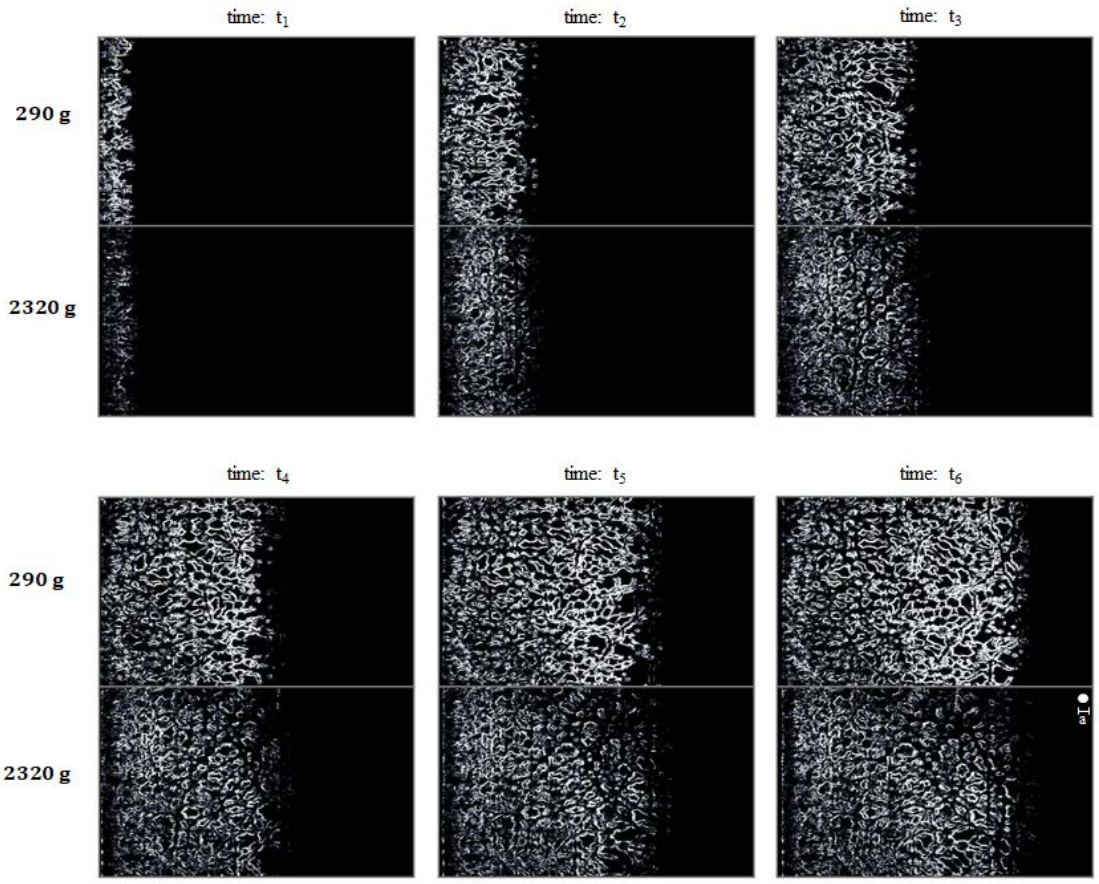

Both waves here are in the shock regime, and they travel at the same speed, independent of confinement.

Figure 13. Sample of force wave images by frame for differing confinements

D. LINEAR REGIME IN SOFT PARTICLES

Past study has shown that force propagation in granular media is separated into two distinct regimes based on initial confinement and impact speed. A shock regime emerges when the forces (or pressure) inside the induced wave are much larger than the ambient conditions in the system (prior to impact). In this regime, the shock (wave) velocity scales with impact as discussed in previous chapters. However, a linear regime has also been shown to exist when the initial contact forces (or ambient system pressure) are much larger than forces inside the induced wave. In this case, the force wave propagates at the speed of sound and does not depend on impact velocity. The results from the 2D simulations and 3D experiments shown in Figures 2 and 4 clearly show this linear regime where the wave speed is roughly constant. Their results confirm that this regime is governed by the initial confinement of the system. It is also important to point out that Dr. Clark's 2D experiments were conducted without initial confinement where no internal sound speed exists and therefore only a shock regime is present. Our experiment uses the same photoelastic particles used by Dr. Clark to study the effects of confining pressure on force propagation. As shown in Figure 12, although we are able to confirm the shock scaling behavior in these soft particles, we are not able to clearly identify a linear regime. The data points for the two smallest impacts ($u_p = 0.12 \text{ and } 0.24$ m/s) show the wave speed to be roughly constant for the 1160 g confinement. This would agree with the fact that larger confinements require faster impacts to transition between the linear and shock regimes. However, in our data the largest confinement (2320 g) appears consistent with the shock scaling behavior identified previously. Additionally, we would expect the wave speed to be faster in the 2320 g confinement (vs the 1160 g) since the wave speed increases with confining pressure in the linear regime (but not in the shock regime). These discrepancies may largely be a result of the data noise that results from difficulty in determining a brightness threshold that is applicable to all experimental parameters as discussed in our data analysis. However, it is also possible that a linear regime may be more difficult to access for soft, highly deformable particles, due to dissipation, viscoelasticity, or other effects.

Based on the transition point for the two regimes, we again make use of the image processing and stacking method discussed in the last section to further investigate the largest confinement case. As shown in Figure 14, for at least one set of trials we are able to successfully extract a wave image whose speed appears relatively constant for the two smallest impacts. This suggests that there may indeed be a linear regime that isn't clearly visible due to the amount of data variance. However, we are not able to successfully reproduce this result for all five sets of trials. We therefore do not conclude definitively that a linear regime is present for these soft particles and further study is required.

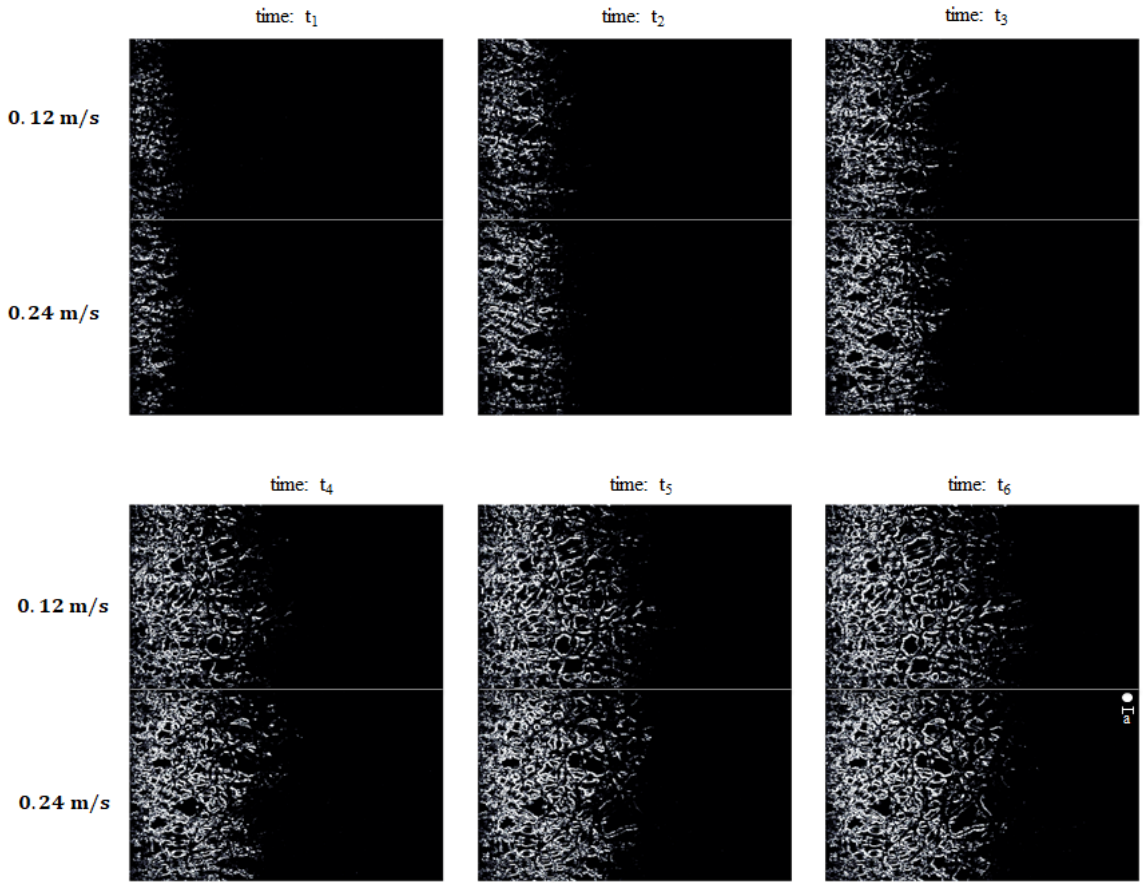

Both waves appear to move at the same velocity, suggesting a linear regime may be present.

Figure 14. Sample of force wave image by frame for differing impact velocities

THIS PAGE INTENTIONALLY LEFT BLANK

VII. CONCLUSION

In this study we examined shock propagation behavior in granular materials through quasi-2D shock experiments of frictional, deformable grains. Using photoelastic techniques we were able to capture system wide grain-scale force information about how a granular medium responds to impacts of varying speed. Through this method we investigated how the shock scaling behavior in soft, highly deformable grains adhere to existing models based on simulations and experimental results in 1D, 2D and 3D systems. Based on our experiments results we produced four key findings: 1) Two distinct wave speeds are visible after impact, where the speed and scaling dependence suggests that the initial regime may correspond with the internal sound of a grain; 2) We are able to clearly identify shock velocities that follow existing scaling models, even in soft grains which are highly deformable; 3) In the shock regime, the wave speed is independent of initial confinement and fall along a single branch; 4) We are not able to clearly identify a linear regime for these soft disks, though we also do not rule out that one is present.

These experimental findings confirmed many expected behaviors; however, a number of questions also arose from the results. We have therefore identified three topics for future study: 1) Can a regime be identified where the wave speed is constant in soft, highly deformable grains? 2) Does the shock scaling behavior change as the wave speed approaches the internal sound speed of an individual grain? 3) Is it possible to observe this internal sound speed using photoelastic techniques during shock experiments?

THIS PAGE INTENTIONALLY LEFT BLANK

LIST OF REFERENCES

[1] K. L. Johnson, *Contact Mechanics*, Cambridge, England: Cambridge University Press, 1987, pp. 84–106.

[2] S. van den Wildenberg, R. van Loo and M. van Hecke, "Shock waves in weakly compressed granular media," *Physical Review Letters,* vol. 111, no. 21, p. 218003, 2013.

[3] F. da Cruz, S. Emam, M. Prochnow, J.-N. Roux and F. Chevoir, "Rheophysics of dense granular materials: Discrete simulation of plane shear flows," *Physical Review E,* vol. 72, no. 02, p. 021309, 2005.

[4] E. Owens and K. Daniels, "Sound propagation and force chains in granular materials," *Europhysics Letters,* vol. 94, no. 5, p. 54005, 2011.

[5] A. Clark, A. Petersen, L. Kondic and R. Behringer, "Nonlinear force propagation during granular impact," *Physical Review Letters,* vol. 114, no. 14, p. 144502, 2015.

[6] C. Daraio, V. Nesterenko, E. Herbold and S. Jin, "Strongly nonlinear waves in a chain of Teflon beads," *Physical Review E,* vol. 72, no. 01, p. 016603, 2005.

[7] C. Daraio, V. Nesterenko, E. Herbold and S. Jin, "Tunability of solitary wave properties in one-dimensional strongly nonlinear phononic crystals," *Physical Review E,* vol. 73, no. 02, p. 026610, 2006.

[8] C. Daraio, V. Nesterenko, E. Herbold and S. Jin, "Strongly nonlinear wave dynamics in a chain of polymer coated beads," *Physical Review E,* vol. 73, no. 02, p. 026612, 2006.

[9] L. Gomez, A. Turner, M. van Hecke and V. Vitelli, "Shocks near jamming," *Physical Review Letters,* vol. 108, no. 05, p. 058001, 2012.

[10] K. Daniels, J. Kollmer and J. Puckett, "Photoelastic force measurements in granular materials," *Review of Scientific Instruments,* vol. 88, no. 05, p. 051808, 2017.

THIS PAGE INTENTIONALLY LEFT BLANK

INITIAL DISTRIBUTION LIST

1. Defense Technical Information Center
   Ft. Belvoir, Virginia

2. Dudley Knox Library
   Naval Postgraduate School
   Monterey, California